3-D modeling of perimeter recombination in GaAs diodes and its influence on concentrator solar cells

M. Ochoa , C. Algora, P. Espinet-González, I. García

ABSTRACT

This paper describes a complete modelling of the perimeter recombination of GaAs diodes which solves most unknowns and suppresses the limitations of previous models. Because of the three dimensional nature of the implemented model, it is able to simulate real devices. GaAs diodes on two epiwafers with different base doping levels, sizes and geometries, namely square and circular are manufactured. The validation of the model is achieved by fitting the experimental measurements of the dark IV curve of the manufactured GaAs diodes. A comprehensive 3-D description of the occurring phenomena affecting the perimeter recombination is supplied with the help of the model. Finally, the model is applied to concentrator GaAs solar cells to assess the impact of their doping level, size and geometry on the perimeter recombination.

1. Introduction

Perimeter recombination must be mitigated in order to increase the efficiency of III–V concentrator solar cells. Because of the complexity of the triple junction solar cells (GaInP/GaInAs/Ge), it is recommendable to start analysing each subcell independently. So far, the most studied subcell has been the middle cell by analysing the GaAs single junction diode [1–4]. It must be taken into account that because of the negligible composition of indium (1–2%) of the GaInAs middle cell, the analysis of single junction GaAs cells grown on GaAs substrates is a valid approach in order to extract conclusions for the triple junction cells. In addition to the usefulness of understanding the GaAs cell perimeter recombination for multijunction solar cells, the recent proposal of using GaAs single junction solar cells for competitive cost of photovoltaic electricity [5] adds interest to this study. It is well known that, as the perimeter-area (P/A) ratio increases, the perimeter current reaches significant values that can lead to a decrease in the open circuit voltage and to an important contribution to degradation mechanisms in GaAs solar cells [1]. Therefore, the performance of small size solar cells such as the most ones used in concentration applications can be affected by perimeter recombination. For example, for modern GaAs solar cells, chemical treatments have been proposed [6] in order to decrease the impact of perimeter recombination.

The dominant sources of perimeter recombination are the surface states. Their main origin comes from dangling bonds at the surface and their formation is due to the loss of periodicity in the crystal (surface states are also created in between interfaces in the crystal and metal-semiconductor contacts but, in this paper we will refer to surface states just at the perimeter of the whole structure). The formation of surface states is very dependent on the mesa-etching process, crystal orientation, surface oxidation, adsorption of impurities at the surface, among others. The surface states energy levels can have a strong effect on the electrical characteristics of the semiconductor because the ionic charges on or outside the semiconductor surface induce image charges in the semiconductor causing the formation of the so-called surface channel or surface depletion-layer which is a region where minority carriers can be confined. Once this channel is formed it gives rise to a surface leakage current [7].

Perimeter recombination in GaAs diodes, transistors and solar cells has been experimentally analyzed and modeled by using 1-D and 2-D (one and two dimension) approaches by several authors [1–4,8,9]. The first approximation to describe this phenomenon was made by Henry et al. [8]. They proposed an analytical expression (1) to obtain the perimeter current assuming: (a) Fermi level pinning and (b) constant electron and hole densities at the surface.

$$J_{per} = qS_0 L_s n_i e^{qV/2kT} \quad (1)$$

where S_0 is the called *intrinsic surface recombination velocity* which is mainly determined by the density of surface states and their capture cross-sections. L_s is the *surface diffusion length* and characterizes carrier injection and recombination in the surface channel.

For Henry et al. the perimeter recombination is controlled by recombination in the *surface channel* (originated to preserve the surface charge neutrality) outside the region where the junction space charge layer intersects with the perimeter and has a $2kT$-behaviour at low forward bias. Later the bias dependence of the ideality factor was studied by Tiwari et al. [9] showing that perimeter recombination exhibits a $2kT$-dependence close to the junction but a kT-dependence in the quasi-neutral regions.

Dodd et al. [2] calculated an effective width (where the perimeter recombination occurs) as a function of the electric field at the surface. Then, the perimeter recombination current was obtained by integrating the recombination rate (obtained numerically) all over the diode's perimeter [2]:

$$I_p = qP\int R_s(y)dy \approx qn_iS_0L_sP\left(e^{qV/nkT}-1\right) \quad (2)$$

where P is the diode perimeter, L_s is the effective width for surface recombination, $S_0=\sqrt{S_{n0}\cdot S_{p0}}$ the recombination velocity of carriers at the surface and n the ideality factor associated with the perimeter current. Dodd et al. also showed that most of the recombination with $2kT$ behaviour took place at low biasing where the space-charge region intersected the perimeter. At higher biasing, the carriers injected in the quasi-neutral regions diffused toward the perimeter where they are recombined. Under that condition the perimeter current ideality factor decreases.

Then, Mazhari et al. made some corrections to the Henry model and got and analytical equation to describe the contribution of the quasi neutral regions to the perimeter recombination. They stated that the kT-behaviour assumed at high forward bias is not always correct and depends on the surface recombination velocity, the doping level and the conductivity of the regions (n or p) [3]. Mazhari et al. did not predict the current dependence on the doping level, just the nkT-behaviour.

Finally, Belghachi et al. [4] calculated separately the contribution to perimeter recombination current from the space charge region (analytical approach) and from the quasi neutral regions (numerical approach). For the contribution of the space charge region, they used the well-known expression for the perimeter recombination current (2) and they made an approximation to calculate the electric field. Regarding the perimeter recombination in the neutral region, they numerically solved the bi-dimensional steady state electron and hole continuity equations. In order to get the perimeter current they added the contribution from the space charge region and that of the quasi neutral regions.

In spite of all these studies, the perimeter recombination is still a phenomenon whose origins are not well known. Therefore, a general model with the following characteristics is required: (a) lack of any restrictive assumption about external conditions such as current flows, voltage range, etc., (b) consideration of any kind of semiconductor structure: n/p or p/n, different doping levels and thicknesses of the layers, etc., (c) 3-D (three dimensional) nature in order to evaluate real device characteristics such as geometry (circular, square, etc.), size, etc. Besides, a model with these characteristics would be able to show the real origins of perimeter recombination and would help to mitigate it.

Accordingly, this paper presents a model for the perimeter recombination of GaAs diodes and consequently, solar cells with those requested characteristics. The model has a 3D nature which is useful to take into account real geometrical effects and to explain the phenomena occurring at different places of the GaAs diode. Besides, n/p GaAs diodes of different P/A ratios, geometries and base doping levels are manufactured in order to analyze the perimeter recombination effects and to validate the model. Finally, simulations of the GaAs solar cell performance as a function of doping level, size and shape (square and circular) are carried out.

Table 1
Structure of n/p GaAs diodes for the two epiwafers, A and B.

Layer	Material	Thickness (μm)	Doping (cm^{-3})	
			A	B
CAP	GaAs:Te	0.17	1×10^{19}	
	GaAs:Te	0.33	1×10^{18}	
Window	$Al_{0.7}Ga_{0.3}As$:Si	0.04	1×10^{18}	
Emitter	GaAs:Si	0.167	1.5×10^{18}	
Base	GaAs:Zn	3.5	3.5×10^{17}	6×10^{16}
BSF	$Al_{0.35}Ga_{0.65}As$:C	0.152	2×10^{18}	
Buffer	GaAs:Zn	1.16	2×10^{18}	
Substrate	GaAs:Zn	350	2×10^{18}	

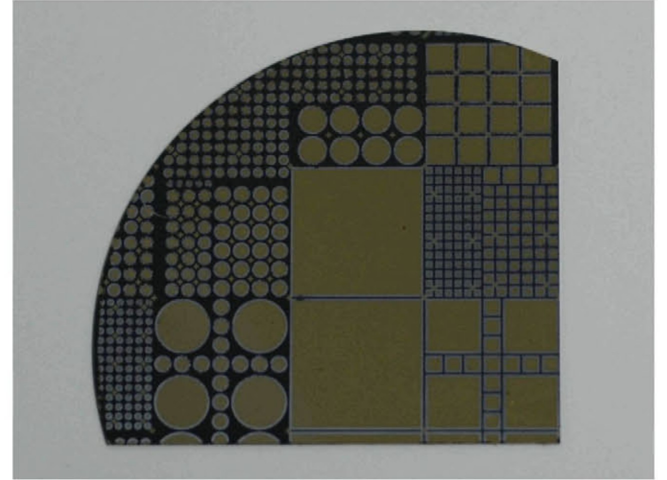

Fig. 1. Picture of the resulting square and circular GaAs diodes with different P/A ratios on a 2-in. wafer portion.

Table 2
Geometrical characteristics of the square and circular diodes manufactured.

Perimeter (cm)		Area (cm^2)		P/A (cm^{-1})
Square	Circular	Square	Circular	Square and Circular
1.6	1.257	0.16	0.126	10
0.8	0.628	0.04	3.14×10^{-2}	20
0.4	0.314	0.01	7.85×10^{-3}	40
0.3	0.236	5.63×10^{-3}	4.42×10^{-3}	53.3
0.2	0.157	2.5×10^{-3}	1.96×10^{-3}	80
0.1	0.078	6.25×10^{-4}	4.91×10^{-4}	160

2. Experimental

Two GaAs concentrator solar cell epiwafers, namely A and B were grown by MOVPE (Metal Organic Vapour Phase Epitaxy). Their structural characteristics are presented in Table 1. The only nominal difference between them is the base doping level. Front metallization was done by Au/Ge, Ni, Au evaporation while Au/Zn/Au were evaporated at the back contact. Both contacts were annealed in order to achieve ohmic contacts and they covered the whole surface of both sides in order to avoid crowding effects and to have a front metal close to an equipotential situation. After the ohmic contact formation, the isolation of individual diodes were achieved by defining mesas using a NH_4:H_2O_2:H_2O 2:1:10 solution. Circular and square GaAs diodes with different P/A ratios were manufactured as shown in Fig. 1 and Table 2.

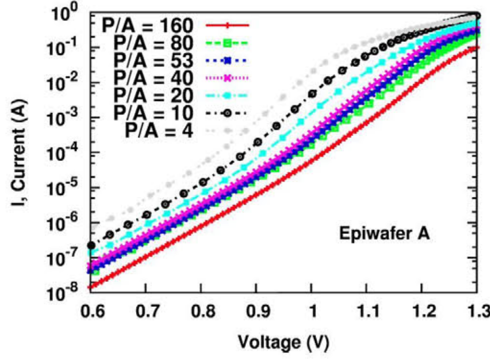

Fig. 2. Experimental dark I–V curves of square diodes for different (P/A) ratios of epiwafer A.

Table 3
Common material parameters used for all simulations.

Parameter	Reference
Band parameters	[11,12]
Bandgap narrowing	[13]
Conduction band discontinuity $Al_xGa_{1-x}As/GaAs$	[12]
Radiative recombination coefficients	[14]
Auger recombination coefficients	[11,12]
Carrier mobilities in GaAs	[15,16]
Carrier mobilities in AlGaAs	[11,12]

After the diode manufacture, the dark I–V curves were measured using a conventional source-meter equipment. In order to measure the I–V curve of a diode, typically the source-meter is swept to a range of voltage and measures the resulting current. Four-wire technique was employed to avoid power loss due to wiring. The diodes were measured on a Peltier system to control their temperature in order to prevent voltage variations due to heating. The resulting dark I–V curves for several representative diodes of epiwafer A are shown in Fig. 2.

3. Theoretical model

The modelling was carried out with the help of the Atlas software from Silvaco [10]. Atlas is a physically based 2-D and 3-D device simulator used to describe the physical behaviour of semiconductor devices. It solves semiconductor fundamental equations derived from Maxwells laws, namely the Poissons equation, the two steady-state continuity equations and the transport drift-diffusion equations. These equations need as input data a careful selection of many material parameters (see Table 3) and models. In this work the following material parameter models and approaches are used:

1. Fermi statistics for carrier concentration calculation are used and all impurities are considered ionized [10].
2. Carrier mobility is calculated with the Klaassen models [15,16]. This model provides a unified description of majority and minority carrier mobilities. It includes the effects of lattice scattering, impurity scattering (with screening from charged carriers), carrier–carrier scattering, and impurity clustering effects at high concentration of impurities. In addition, it is a model designed for device simulation and it has been calibrated for a wide range of temperatures for silicon. In order to properly use the Klaassen mobility model it has to be carefully calibrated for GaAs materials. We performed this calibration by fitting the results to other well-accepted mobility models for GaAs structures at room temperature [17–19].
3. Band gap narrowing due to heavy doping is also taken into account [13]. The band gap shrinkage in GaAs has been demonstrated to be important in order to reproduce measured data and it has a significant impact on p-GaAs while on n-GaAs its impact could be masked by degeneration effects [20].
4. Band to band radiative and Auger recombination models presented in [10].
5. The Shockley–Read–Hall recombination (from now on, SRH) is calculated in the bulk and at the surface.

Regarding surface states, we use based-trap centres SRH recombination (same approach as bulk) to calculate their contribution to the dark I–V curves. Although surface states could have multiple levels lying inside the forbidden gap, a single-level model is useful enough to describe their impact on the device behaviour. This can be implemented in two ways: (1) by reducing the carrier lifetimes by assigning an effective surface recombination velocity (SRV-model) and (2) by modifying the charge density at the surface by adding a specific density of traps (Trap-model). We have proved that both approaches are valid in order to model surface recombination in agreement with [2], but significant basic differences exist by using one or another. In fact, the presence of surface traps (Trap-model) creates an additional space charge region along the surface (neglected by the SRV-model) which alters the electrical interaction of carriers which can be important if the device is analyzed under different external conditions. Therefore, the Trap-model helps to describe more accurately the mechanisms behind by providing more insights to perimeter recombination so, it is the model chosen in this paper to analyze the origin of perimeter recombination in GaAs diodes and solar cells.

The Trap-model takes into account that carriers are being emitted or captured by donor or acceptor-like traps lying in the forbidden gap. This interaction exchanges charge between conduction and valence bands so, the charge density at the surface is modified according to

$$div(\epsilon\nabla\psi) = q(n-p-N_D^+ + N_A^- + N_{tD}^+ - N_{tA}^-) \quad (3)$$

where ψ is the electrostatic potential, ϵ the local permittivity, N_D^+ and N_A^- are the densities of ionized donor and acceptor impurities respectively, N_{tD}^+, N_{tA}^- are the ionized trap density for donors and acceptors and the other variables have their usual meaning. The ionized trap densities depend upon the trap density, N_{tD} and N_{tA}, and its probability of ionization, F_{tD} and F_{tA}. For donor-like and acceptor-like traps respectively, the ionized densities are: $N_{tD}^+ = N_{tD} \times F_{tD}$ and $N_{tA}^- = N_{tA} \times F_{tA}$.

The probability of ionization assumes that the capture cross-sections are constant for all energies in a given band and follows the analysis developed by Simmons and Taylor [21]. The initial occupancy of traps is calculated by the following equations for acceptor and donor-like traps:

$$F_{tA} = \frac{\upsilon_n\sigma_n n + e_{pA}}{\nu_n\sigma_n n + \nu_p\sigma_p p + e_{nA} + e_{pA}} \quad (4)$$

$$F_{tD} = \frac{\upsilon_p\sigma_p p + e_{nD}}{\nu_n\sigma_n n + \nu_p\sigma_p p + e_{nD} + e_{pD}} \quad (5)$$

where σ_n and σ_p are the carrier capture cross-sections for electrons and holes, respectively and ν_n and ν_p are the thermal velocities for electrons and holes. The probability of ionization (Eqs. (4)–(5)) is the electron–hole concentration to the total carrier concentration ratio which are determined by the electron emission rate e_{nD} and the hole emission rate e_{pD}. For donor like traps, the electron and

hole emission rates, respectively are defined by

$$e_{nD} = \frac{1}{g} \upsilon_n \sigma_n n_i \exp\left(\frac{E_t - E_i}{kT}\right) \tag{6}$$

$$e_{pD} = g \upsilon_p \sigma_p n_i \exp\left(\frac{E_i - E_t}{kT}\right) \tag{7}$$

where g is the degeneracy factor of the material, n_i the intrinsic carrier concentration, E_t the trap energy level, E_i the intrinsic Fermi level and the other variables have their usual meaning. For acceptor like traps, the term e_{nA} and e_{pA} are the electron and hole emission rates defined by

$$e_{nA} = g \upsilon_n \sigma_n n_i \exp\left(\frac{E_t - E_i}{kT}\right) \tag{8}$$

$$e_{pA} = \frac{1}{g} \upsilon_p \sigma_p n_i \exp\left(\frac{E_i - E_t}{kT}\right) \tag{9}$$

The above equations help us to define the charge density at the surface and they modify the carrier concentration. This modification is implemented in the recombination term for both carrier types as

$$R_n = \frac{np - n_i^2}{\tau_n \left[p + g \cdot n_i \exp\left(\frac{E_i - E_t}{kT}\right)\right] + \tau_p \left[n + \frac{1}{g} n_i \exp\left(\frac{E_t - E_i}{kT}\right)\right]} \tag{10}$$

for donors and

$$R_p = \frac{np - n_i^2}{\tau_p \left[n + \frac{1}{g} n_i \exp\left(\frac{E_t - E_i}{kT}\right)\right] + \tau_n \left[p + g \cdot n_i \exp\left(\frac{E_i - E_t}{kT}\right)\right]} \tag{11}$$

for acceptors. The carrier lifetime $\tau_{p,n}$ is derived from the defect density and is equal to $\tau = (\sigma \nu_{th} N_t)^{-1}$. Here N_t is the trap density, ν_{th} the carrier thermal velocity and σ the capture cross-section.

The recombination terms are added to the carrier continuity equations in order to solve self-consistently the semiconductor fundamental equations to calculate dark I–V curves. A similar but less accurate approach of modelling perimeter recombination has been successfully employed in the past by Dodd et al. [2]. The Dodd's work has a 2-D nature and lacks of series resistance consideration. Therefore, in order to get the most accurate results of real devices simulations, a 3-D model becomes a need to reproduce the whole dark I–V curve in GaAs diodes. So, our model is able to fit the experimental dark I–V curves of real GaAs diodes (including series resistance). Accordingly, we have simulated devices with different shapes, sizes and doping levels.

3.1. Simulation environment

Atlas 3-D simulator is based on prismatic meshes and has been developed from 2-D codes that use triangular meshes, this means that the third dimension is created by a stack of 2-D slices extended in the z-direction. Dealing with a 3-D problem involves a number of equations at least one order of magnitude greater than a 2-D problem [22]. For large problems as in our case (greater than 5000 grid points), iterative and direct solvers can be used. In this study, we have used iterative solvers due to the lower solution time and memory usage [10,22].

One of the main issues in multi-dimensional device simulation is the mesh definition or gridding. In drift-diffusion models, the calculation of perimeter recombination is very dependent on the mesh resolution. The mesh spacing near the surface must be as low as possible, otherwise, the influence of perimeter recombination in the dark I–V curve will be overestimated. In fact, the mesh size must be lower than the semiconductor Debye length to properly resolve charge variations in space [23]. At 300 K, the Debye length for GaAs materials with doping level of 4×10^{18} is about 2 nm. This doping level corresponds to the highest one used for the pn junctions of this work.

In order to provide a high-degree of accuracy, the final value of mesh spacing (1 nm) was obtained by reducing the mesh spacing until no significant changes in the potential at the surface were observed which turns in a negligible impact on the calculated I–V curves. This value (1 nm) meets the requirement of the Debye length and provides high-degree of accuracy in drift-diffusion models.

3.2. Validation of the model

In order to validate the model, it has to be capable to describe the experimental behaviour of perimeter recombination in GaAs diodes. This has been done by analysing how the model is going to behave while the constants or parameters are tweaked. The model has several adjustable input surface parameters: N_t, σ, E_t and g for both electrons and holes and for each type of trap (donor-like or acceptor-like). We have analyzed the influence of each parameter in the dark I–V curve. We have verified by simulations that the impact of degeneracy factor and trap energy level (within a reasonable range) can be considered negligible for these devices so, all simulations were performed with a trap level located at the mid-gap in agreement with [2]. On the other hand, the densities of traps and capture cross-sections have a strong influence on the I–V curve as Fig. 3 shows for N_t variations. As can be seen in Fig. 3 perimeter recombination influence can be extended to high bias if N_t is high enough. This is a result not shown in previous works. Conversely, if the capture cross-sections (not shown here) are increased it is also possible to obtain a high impact of perimeter recombination.

The model validation was carried out by fitting experimental dark I–V measurements such as those of Fig. 2 to the model. Accordingly, Fig. 4a and b shows the fitting achieved for square and circular devices for epiwafer A for three different P/A ratios while Fig. 4c shows the fitting achieved for square devices for epiwafer B. It is remarkable that for both Fig. 4a and b the only changed parameters for different diodes were their size and shape, while the rest of surface and bulk parameters were kept constant (see Tables 3 and 4). Conversely, the only changed parameters for different diodes in Fig. 4 were their size and shape. Because epiwafers A and B have different doping levels, thus different bulk trap densities have been used for Fig. 4a, b and c and their values are very similar to those found in [24].

The surface trap parameters (similar to those found in [25]) are the same for A and epiwafer B indicating that our mesa-etching process (same for both) is not sensitive to the base doping level analyzed. The most reasonable values of trap parameters at surface and bulk were extracted by using a Levenberg–Marquardt algorithm [26] and they are listed in Table 4. As a result, Fig. 4 shows that the model is able to simulate the whole I–V curves with high accuracy.

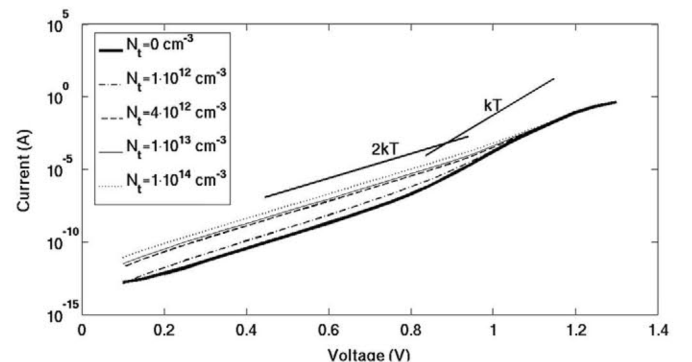

Fig. 3. Influence of surface trap densities N_t on the dark I–V curve for P/A=40.

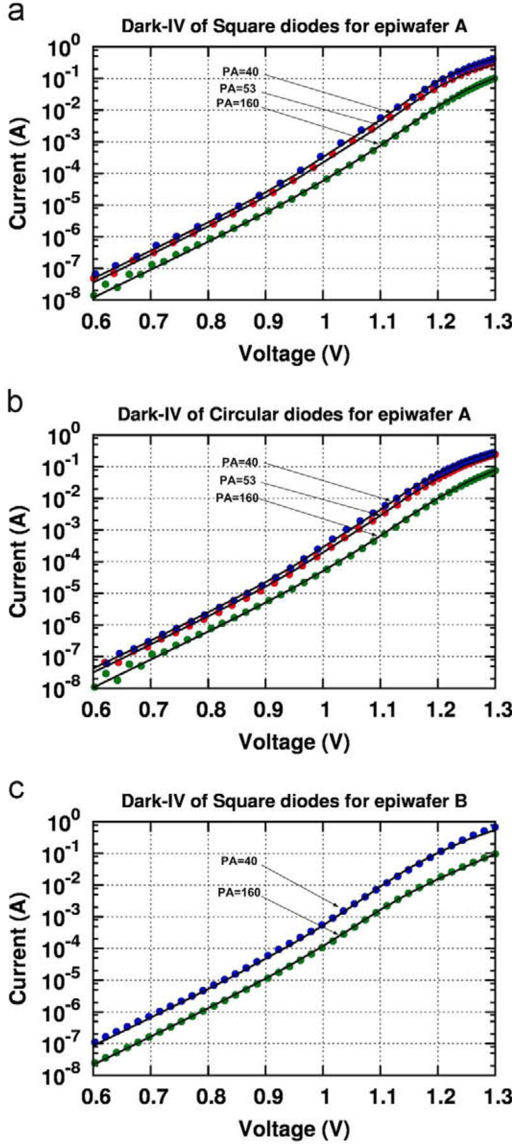

Fig. 4. Data fitting for: (a) square devices and (b) circular devices for epiwafer A with P/A = 160, 53, 40 – in blue, red and green, respectively, and (c) square devices for epiwafer B with P/A = 160, 40 – in blue and green respectively. Lines are used for simulation and symbols for experimental data.

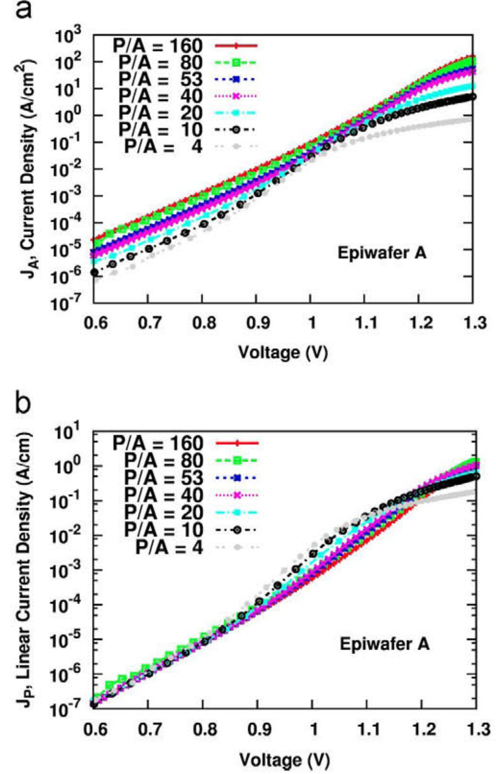

Fig. 5. Dark (a) $J_A - V$ curves and (b) $J_P - V$ curves of square diodes for different (P/A) ratios of epiwafer A.

Table 4
Trap parameters at surface and in bulk used in simulations of diodes manufactured on epiwafers A and B.

Epiwafer	Type	N_t	Energy level	σ_n(cm^2)	σ_p(cm^2)
A, B @Surface	Acceptor	4×10^{12} cm^{-2}	Midgap	8×10^{-15}	8×10^{-15}
	Donor	4×10^{12} cm^{-2}	Midgap	8×10^{-15}	8×10^{-15}
A @Bulk	Acceptor	6×10^{13} cm^{-3}	Midgap	1×10^{-16}	1×10^{-13}
	Donor	6×10^{13} cm^{-3}	Midgap	1×10^{-13}	1×10^{-16}
B @Bulk	Acceptor	3×10^{13} cm^{-3}	Midgap	1×10^{-16}	1×10^{-13}
	Donor	3×10^{13} cm^{-3}	Midgap	1×10^{-13}	1×10^{-16}

4. Discussion

The measurements of the dark I–V curve show the influence of both the area and perimeter in the GaAs diodes. In order to better analyze the dark I–V curves (see Fig. 2) they were transformed into J_A–V curves (A/cm^2) by considering the diode area and J_P–V curves (A/cm) by considering the perimeter length in Fig. 5a and b, respectively. As can be seen, at low bias the current does not correlate with the area while it does with the perimeter so, the perimeter recombination dominates the dark current. At high bias, the results tend to show a mixture of area and perimeter correlation except for $P/A < 40$ which also exhibit a near perimeter dependence. A similar behaviour was found for circular diodes. Manufactured diodes on epiwafer B exhibit perimeter recombination extended to higher biases than those from epiwafer A.

Once we have proved the validity of the model and verified that dark I–V curves are affected by perimeter recombination, we are going to use the model to understand the origin and behaviour of perimeter recombination.

4.1. Origin of perimeter recombination

Surface states at the perimeter of GaAs devices can be partially occupied by adsorbed atoms (such as oxygen, an excess of arsenic, etc.) which set the character and ionization energy of the trap. Since we lack of information about the energy level of the trap and the amount of charged or neutral states at the perimeter, we have set equal trap density and energy level for electrons and holes. Therefore, surface states at the perimeter are able to trap electrons or holes with equal probability so, they can be neutral or charged depending on the position of the Fermi level. For p-type regions the position of the Fermi level lies closer to the valence band than the conduction band, which in fact sets the charge state (neutral or charged) of the traps. In such case, the acceptor-like traps (electron trap) are neutral and the donor-like (hole trap) are positively charged. In order to maintain charge neutrality the same amount of positive surface charge is screened with negative charges in the semiconductor bulk. This accumulation of charges makes the bands to bend downwards. The opposite behaviour applies to the n-type region bending the band upwards. A representative

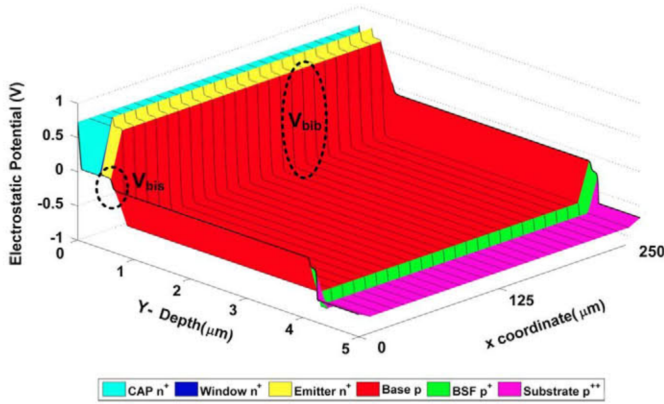

Fig. 6. Simulated 3-D plot of the electrostatic potential at equilibrium in P/A = 160 diodes of the epiwafer A. *X*-coordinate shows a cross-section of the diode where at 0 and 250 μm are placed at the borders of the structure where perimeter recombination appears. *Y*-direction (depth) at distances larger than 5 μm (substrate) is not shown for simplicity. The two dashed ellipses denotes the different potential barriers for carriers (see Fig. 7).

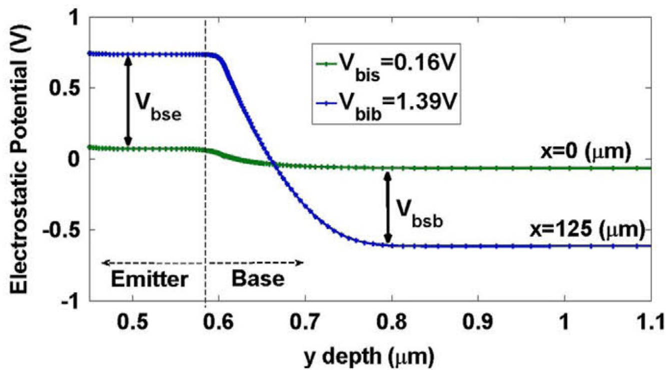

Fig. 7. Zoom of the dashed ellipses of Fig. 6 representing the cutline at perimeter (V_{bis} = 0.16 V, green line) and bulk (V_{bib} = 1.39 V, blue line) in the p–n junction. V_{bse} (0.6 V) denotes the potential barrier seen by a carrier from the emitter bulk to the emitter surface (away from the depletion region where the potential is flat at bulk) if it moves in the same x coordinate. V_{bsb} (0.56 V) is for case in the base region.

picture of this can be found elsewhere [27]. Accordingly, the bending intensity is characterized by a potential (reduced all along the perimeter with respect to bulk) that builds a surface channel where minority carriers are confined.

Fig. 6 shows the impact of the band bending in the electrostatic potential at equilibrium and the comparison between the built-in potential at surface (V_{bis}) and bulk (V_{bib}) of a diode of epiwafer A. The interaction of carriers (mainly minority) with surface traps influences the distribution of the potential barrier V_{bis} at surface which is smaller (0.16 V) than the built-in potential at bulk (1.39 V) so, the potential barrier to be surpassed by carriers at the p-n junction will be lower at surface than in the bulk region (away from the surface). In addition, minority carriers from bulk also find a lower potential (0.56 V from the base to the surface and 0.6 V from the emitter to surface) at the surface away from the intersection of the p-n junction with the perimeter than the one at bulk (V_{bib}). This potential corresponds to the difference between V_{bis} and V_{bib} (see Fig. 7).

The surface channel region is associated to the local curvature of the bands which is proportional to the space charge density created by surface states. This curvature has two major characteristics such as its amplitude and width. The width (distance of the band bending from perimeter into the bulk) extends into the bulk until the band is flat. The wider the surface channel, the greater the space charge region from surface to bulk where minority carriers decrease. In the case of the amplitude of the band bending, the higher its value the easier for carriers to flow to that region.

In Fig. 8 the potential distribution at the p-n junction is shown for three bias voltages. By increasing the forward bias, the voltage applied reduces the built-in potential at bulk and along the surface. Once the voltage bias reaches values above V_{bis}, the p–n junction at the surface is not longer a barrier but an electron sink. This causes the depletion region at the surface to begin to empty reducing the conduction surface channel width and amplitude by lowering its curvature so, the surface potential begins to be comparable to the one in bulk. Even at high bias, there is a lower potential at the perimeter, however, this happens in a very short distance and is no longer significant to the large amount of carriers at the bulk of the device.

The potential shown in Fig. 8 is related to the spatial distribution of charges affecting the carrier concentration, thus, the recombination rate. In Fig. 9 we can confirm the surface channel behaviour under forward bias by analysing the recombination rate at the same portion of the device where the major influence of surface traps takes place. It can be deduced from Figs. 8 and 9 that minority carriers will recombine more at locations where they find the lowest barrier to overcome. The lower barriers are always found at the perimeter of the device but, its contribution to recombination changes according to the bias applied.

If we analyze the recombination rate under forward bias we can see that at any voltage the higher recombination is at the perimeter where the band bending and accumulation of charges is more pronounced. At low bias, there are locations at the perimeter junction and its surroundings with a high recombination rate coming mainly from the space charge regions. This recombination begins to spread into the bulk as the bias voltage is increased. Therefore, at the vicinity of the space charge region at the surface and bulk the recombination rate begin to increase due to the fact that all traps inside the space charge region are ionized so, minority carriers begin to occupy bulk and surface trap states outside the space charge region. The latter makes the contribution of quasi-neutral regions significant as the voltage is increased. Hence, at higher biasing, the surface channel still acts as a sink of carriers but, the difference between bulk and perimeter recombination values is decreased. This reduction is enough to make the integration of recombination rate in bulk regions greater than the one at the surface.

The recombination rate is more extended into the base at bulk and perimeter on epiwafer B than on epiwafer A due to the lower potential barrier found (see Fig. 8). This shows that perimeter recombination also depends on the doping level of the p and n regions. To the best of our knowledge this is the first time that the doping dependence of perimeter recombination is shown theoretically. Due to its importance, doping level is analyzed in the next section.

4.2. *Doping influence*

In the work done by Mazhari et al. [3] the influence of doping level and dopant type was considered but, only affecting the *kT*-recombination region. Nevertheless, we will show below that the doping level could also affect the 2*kT*-recombination region and plays an important role in the formation of the surface channel. In Fig. 10, two representative square diodes of the same size one manufactured on epiwafer A and the other on epiwafer B are compared. The diode manufactured on epiwafer B exhibits more recombination current. This is an interesting result that has not been explained in the past.

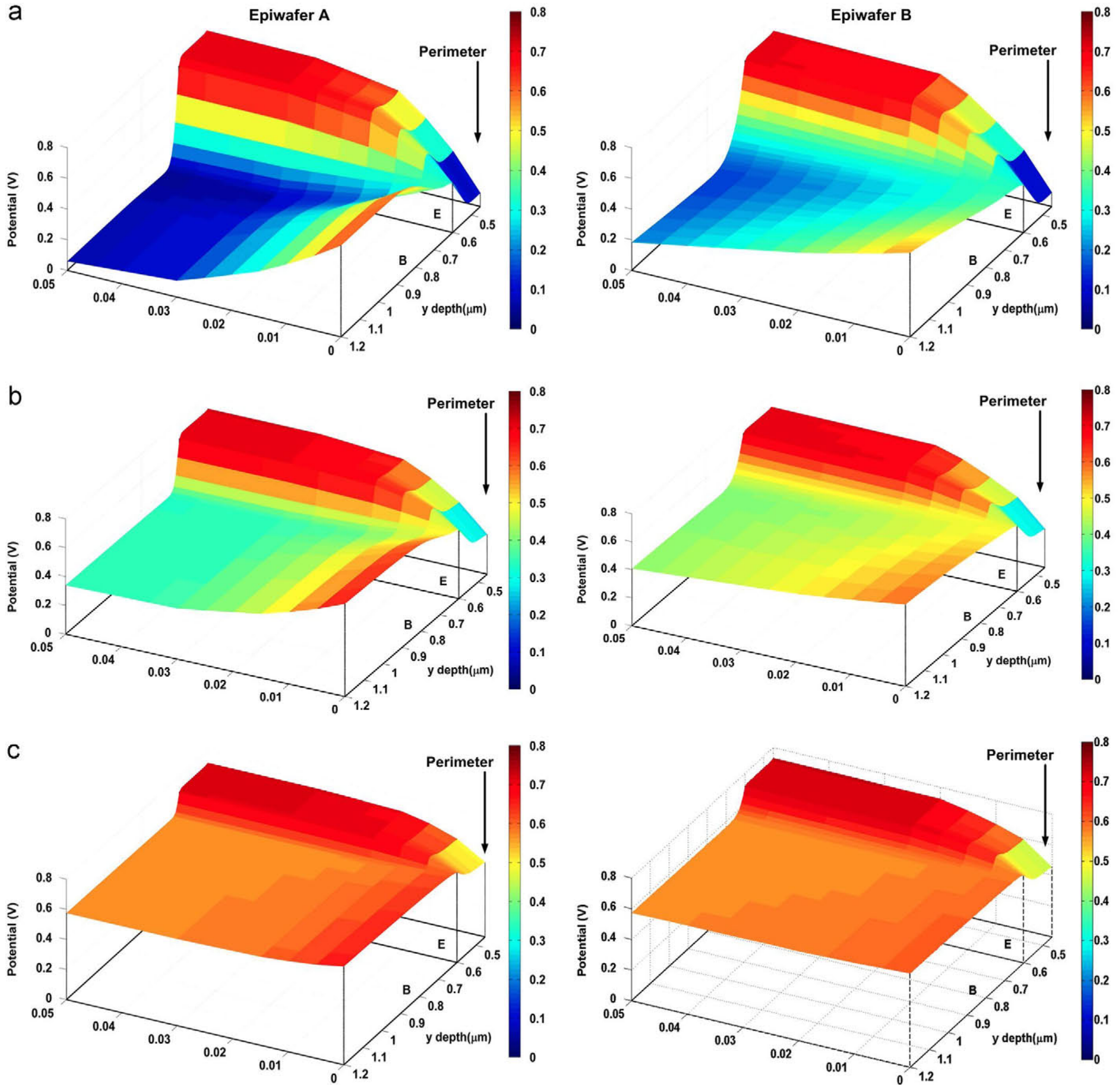

Fig. 8. 3-D plot of the potential at the p-n junction near the surface perimeter ($x = 0$ μm) for epiwafers A (left) and B (right) under forward bias: (a) 0.7 V, (b) 1 V and (c) 1.3 V. The depth and width (along *x*-coordinate) of the structure sides is shortened for simplicity. At the ground of the figures letter *E* denotes emitter while *B* is for base region.

The larger recombination current of diodes of epiwafer B in the whole range of voltage is mainly due to the lower potential V_{bis} at the perimeter. In Fig. 6 the built-in potential at surface for epiwafer A is around 0.16 V which is a very low barrier compared to the 1.39 V built-in at bulk (1.34 V for bulk and 0.14 V for surface for epiwafer B). The different potential distribution is due to the difference in the base doping level, thus, the surface channel characteristics. In the case of epiwafer B the depletion layer from the n-type region (emitter) to the p-type region (base) is more extended into the latter when the doping level of the base is lower. For epiwafer A the surface channel width for the region where the maximum band bending occurs at equilibrium (at the base of the diode) is around 60 nm while for epiwafer B increases to 160 nm. The surface channel of the emitter for both epiwafers is around 70 nm. Therefore, the space charge region created at the surface is larger for diodes of epiwafer B. Consequently, the higher the doping level the higher the amplitude of the bending. The lower the doping level the wider the surface channel. The effect of the wider space charge region in perimeter recombination is shown in Fig. 9. For both epiwafers the higher recombination occurs where the junction space charge region intersects the perimeter as Dodd et al. [2] stated. For epiwafer A the peak of recombination occurs exactly at the intersection of the p–n junction with the perimeter which is not the case for epiwafer B where highest values are found at the p–n junction intersection but the peak is shifted a few nanometres into the base due to the larger space charge region. The same fact applies for the bulk recombination in both sides of the junction. The peak of recombination occurs at the location where there is a maximum availability of carriers (the highest *np* product).

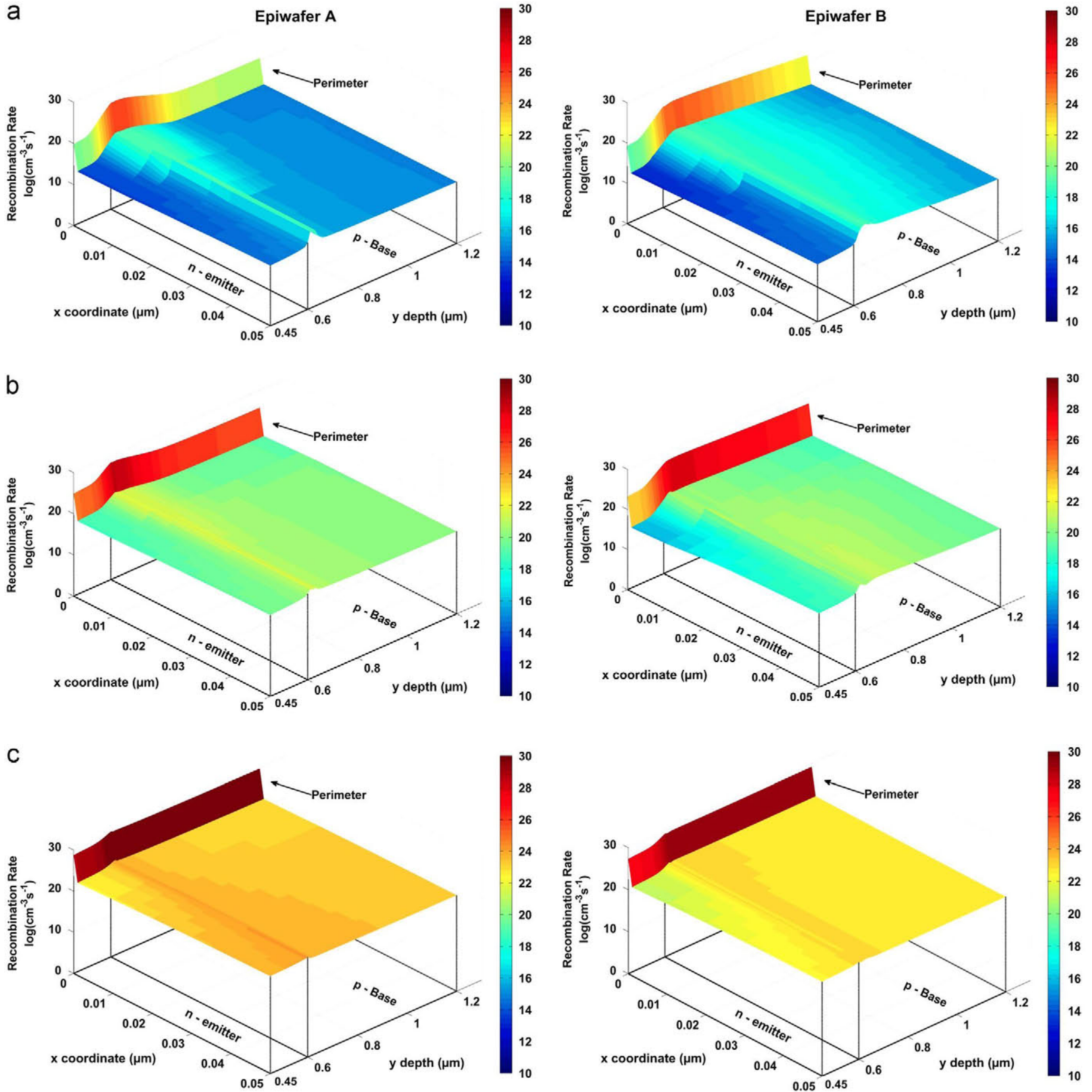

Fig. 9. Semi-logarithmic 3-D plot of recombination rate at the p–n junction for epiwafers A (left) and B (right) under forward bias: (a) 0.7 V, (b) 1 V and (c) 1.3 V. The depth and width (*x*-coordinate) of the structure sides is shortened for simplicity.

In order to know the dominant recombination types, Fig. 11 shows the contribution of some recombination mechanisms as a function of the bias voltage for both epiwafers. As can be seen, perimeter recombination is the dominant till $V = 1.1$ V (A) and $V = 1.2$ V (B). Therefore, perimeter recombination can extend its influence to high voltage biasing being highly dependent on bulk doping level.

4.3. *Influence of perimeter recombination on GaAs concentrator solar cells*

In this section, the model is used to discuss some of the key factors that affect perimeter recombination of GaAs concentrator solar cells. It must be noted that we do not pretend to carry out an exhaustive solar cell optimization but to show some case studies. First, we analyze the influence of p–n junction doping level followed by the size and geometry of the solar cells.

4.3.1. *Doping influence*

The optimum base doping level for GaAs concentrator solar cells is a trade-off between series resistance, recombination current density and photogeneration current. While having a highly doped base provides a low resistivity it will reduce the photogeneration current by decreasing the electron diffusion length (the radiative and SRH lifetimes are better at lower dopant concentrations). Reducing the doping level will increase the electron diffusion length in base, but as we have seen, at low

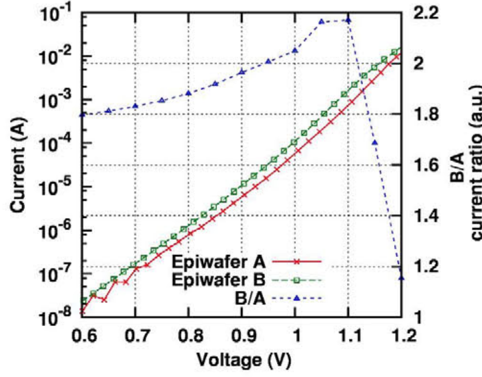

Fig. 10. Experimental measurements of the dark I–V curve for two representative diodes (P/A = 160) manufactured on epiwafers A and B showing the influence of the base doping level. The blue line corresponds to the current ratio of both diodes as a function of the bias. (For interpretation of the references to color in this figure caption, the reader is referred to the web version of this paper.)

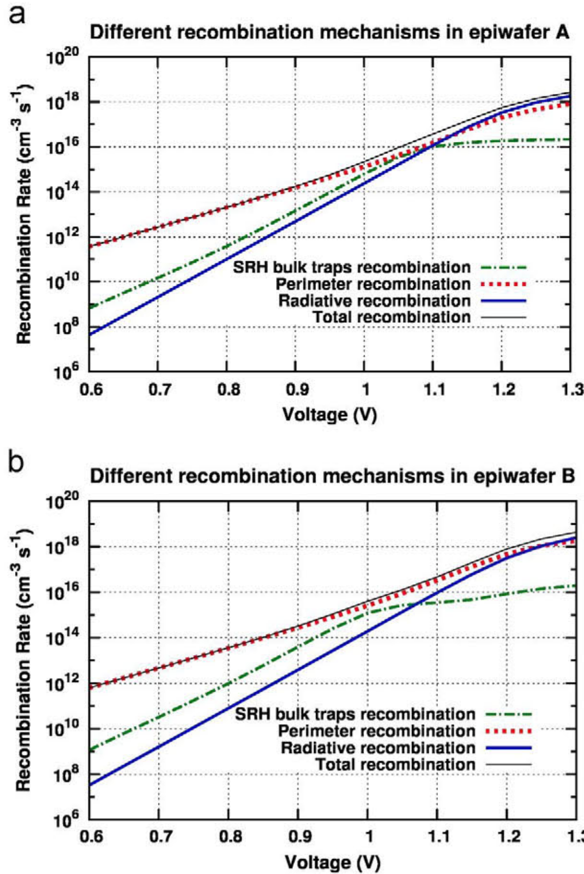

Fig. 11. Simulation of the recombination rate contribution for radiative and non-radiative processes for a P/A=40 diode: (a) epiwafer A and (b) epiwafer B. Auger recombination is negligible with respect to the other recombination mechanisms so, for the sake of simplicity it is omitted.

doping levels perimeter recombination could be important depending on the size of the device. Therefore, a further reduction of the base doping level could be useless without avoiding perimeter recombination.

In order to assess the influence of base doping levels, simulations on a square device of 0.01 cm^2 (P/A=40) were performed from 1×10^{16} cm^{-3} to 4×10^{18} cm^{-3} (Fig. 12) while keeping constant the rest of parameters from Tables 3 and 4. As can be seen, as the doping level increases the recombination current reduces by a factor of 10 (when comparing $N_A = 1 \times 10^{16}$cm^{-3} and

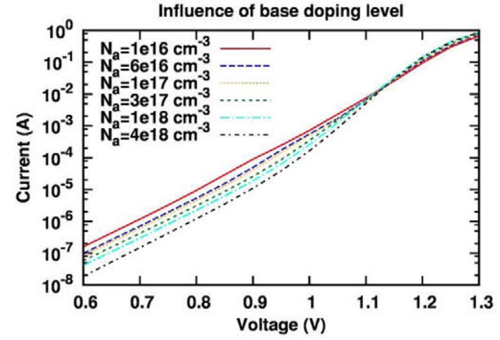

Fig. 12. Simulated dark I–V curve of a GaAs solar cell with a size of 0.01 cm^2 (P/A=40) varying the p-base doping level.

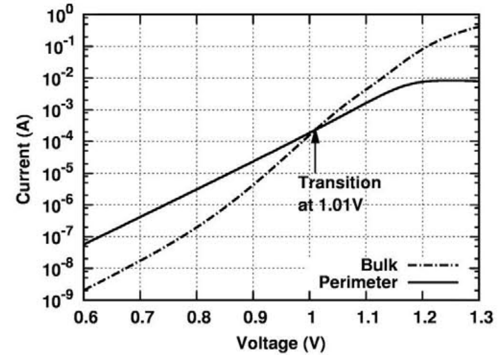

Fig. 13. Simulation of the contribution of bulk and perimeter currents for a solar cell with a size of 0.01 cm^2 (P/A=40) manufactured on epiwafer A.

4×10^{18} cm^{-3}) from low bias until 1.1 V (mainly because of the perimeter recombination influence) and after this value the current increases by a factor of 1.5 (this factor corresponds to the maximum difference at 1.2 V). At high biasing (after 1.1 V), the radiative recombination current is more dominant than the perimeter one while increasing the doping level due to the larger carrier concentration and the reduction of perimeter recombination current (see general trends of Fig. 11). Thereby, when the base doping level is increased the total current approaches to a kT-behaviour because of a dominant radiative recombination component.

In the case of the emitter doping level variation (not shown here) the difference in total current is very low (assuming n/p structures with typical doping levels in base and emitter). Therefore, the main contribution to dark current comes from the base region.

4.3.2. Size influence

In order to quantitatively account for the contribution of perimeter recombination on different solar cell sizes, the boundary condition at the surface (N_t=0, from equation for lifetime values included in Eqs. (10) and (11)) is removed to separate the influence of bulk and perimeter surface current. The evolution of both currents for a P/A=40 (0.01 cm^2) square solar cell is shown in Fig. 13. Table 5 summarizes the transition voltage values where the bulk recombination current equals the perimeter one and where the bulk current becomes dominant being five times greater than the perimeter one.

For smaller sizes of square solar cells the perimeter recombination has a strong influence on the whole voltage range. In fact, the smaller size (6.25×10^{-4}cm^2) analyzed shows that perimeter recombination current is the one that dominates the whole dark I–V curve. Even for larger sizes (1 cm^2 for square solar cells) the

perimeter current dominates until 0.88 V for epiwafer A. In the case of solar cells on epiwafer B even the larger sizes are strongly affected by perimeter recombination.

For concentrator solar cells, the determination of the optimum size is a trade-off between the series resistance, perimeter recombination and the capacity to remove the heat away from the solar cell [28]. Therefore, this study will contribute to such optimization.

4.3.3. Geometry comparison

In order to compare square and circular solar cell geometries in terms of perimeter, it is useful to assign the same area for both geometries. Fig. 14 shows the ratio of the dark current density for square cells to the dark current density for circular cells as a function of the solar cell area for two bias voltages. The voltages considered are not affected by series resistance (omitted) and they are intended to show the performance of solar cells when perimeter recombination dominates (0.7 V) and when they are close to the typical operation point of GaAs solar cells (1 V).

It is important to have in mind that by equating the cell areas of both geometries the perimeter of square ones is $2\Pi^{-1/2}$ times larger than the circular ones. So, it could be expected that the larger perimeter in square cells will exhibit a greater recombination current but Fig. 14 shows the opposite. The reason why circular cells (with shorter perimeter length) are worse in terms of dark current is because the values of the surface traps densities fitted to the experimental data (see Fig. 4) are 1.5 times bigger for circular than square devices (see surface traps values in Fig. 14). This fact counterbalances the effect of a larger perimeter length of square devices.

Therefore, the perimeter recombination of our circular devices is more affected by the mesa-etching process used than the square ones. As Fig. 14 shows, square cells will exhibit less recombination current for any cell size at 0.7 V. At 1 V, the difference between both geometries decreases with the cell area. The reason why at 1 V bias voltage the difference between square and circular solar cells becomes lower than at 0.7 V is the following. At 0.7 V, perimeter recombination dominates (see Fig. 13 and Table 5) for all the considered areas in Fig. 14. However, at 1 V perimeter recombination influence decreases while area dependent recombination mechanisms start to dominate (see Fig. 13) thus, the dashed line of Fig. 14 increases as a function of area and the difference between both geometries becomes lower.

In order to explain why our square devices exhibit a lower trap density than the circular ones, the crystallographic orientation can play a key role. Stellwag [29] showed that perimeter recombination could be reduced if the mesa-isolation process is properly oriented to the crystallographic axes of the device.

Moreover, a given device presents different perimeter properties according to each orientation side of its mesa etching. For square solar cells, two sides are aligned while the other two are misaligned to the crystallographic axes of the wafer, thus, the latter will have higher perimeter recombination values. In the case of circular devices, the orientation to crystallographic axes is not well defined due to its inherent geometry. Only a small portion of the perimeter could be completely oriented (much lower than square shapes) to the crystallographic axes. A lower perimeter recombination for square devices than for circular ones was also found in [30].

It should be pointed out that the model used is able to take into account indirectly the orientation-dependence. For example, in square devices, the same fit to experimental data is achieved with surface trap densities around 5 times lower for the $01\overline{1}$ oriented sides than for the 011 oriented ones. This difference factor in the perimeter properties for the angle of orientation is in agreement with previous experimental work [29].

Table 5
Voltage values where bulk current (I_b) is equal and five times greater than perimeter current (I_p) for different solar cell sizes.

P/A (cm^{-1})	Area (cm^2)	Voltage (V)			
		$I_b = 5{*}I_p$		$I_b = I_p$	
		A	B	A	B
160	0.00625	> 1.3	> 1.3	1.229	1.264
40	0.01	1.264	> 1.3	1.011	1.229
13	0.09	1.205	1.271	0.929	1.191
10	0.16	1.183	1.26	0.913	1.178
5	0.64	0.999	1.233	0.899	1.121
4	1	0.992	1.224	0.88	1.097

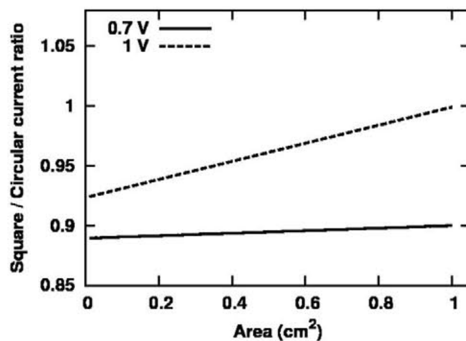

Fig. 14. Simulated circular dark current density to square dark current density ratio as a function of the solar cell area (the same for both geometries). Two bias voltages (0.7 and 1.0 V) are considered. The surface traps densities for circular and square devices are 4×10^{12} cm^{-2} and 6×10^{12} cm^{-2} respectively.

5. Summary and conclusions

A 3D model for the perimeter recombination in GaAs diodes and solar cells has been presented. The model assumes the variation of the charge density at the perimeter surface by considering a given density of traps. Additionally, GaAs diodes on two epiwafers with different base doping levels, sizes and geometries, namely, square and circular have been manufactured. An excellent fitting of the experimental dark IV curves of these diodes is used to validate the proposed model. By using the model, it is found that a surface channel region with a width of some tens of nanometers is proportional to the space charge density created by perimeter surface states. The model is able to explain why the perimeter recombination is dominant at low biasing but it can be also very influencing at high biasing. Detailed 3-D figures of electrostatic potential and recombination rates are supplied for the real devices manufactured. An interesting result is the explanation of the influence of the bulk doping level on the perimeter recombination which is experimentally found in the manufactured GaAs diodes. Finally, the 3D model is used to analyze the influence of doping level, size and geometry (square and circular) on the perimeter recombination affecting GaAs concentrator solar cells. As a result, it is found that small solar cells can be influenced by perimeter recombination even beyond the typical operation point of concentrator cells (about 1 V) and that square cells exhibit a lower perimeter recombination than circular ones. In any case, the control of the doping level can be used as one of the ways to decrease perimeter recombination.

Acknowledgments

This work has been supported by the Spanish Ministerio de Economía y Competitividad with the project TEC2011-28639-C02-01, IPT-2011-1441-920000 and IPT-2011-1408-420000, as well as the Comunidad de Madrid under the NUMANCIA II programme (S2009/ENE1477) and by the European Commission under the project NGCPV "A new generation of concentrator photovoltaic solar cells, modules and systems" with Grant agreement no. 283798.

References

[1] P. Espinet, C. Algora, J. González, N. Núñez, M. Vázquez, Degradation mechanism analysis in temperature stress tests on III–V ultra-high concentrator solar cells using a 3D distributed model, Microelectronics Reliability 50 (2010) 1875–1879.

[2] P. Dodd, T. Stellwag, M. Melloch, M. Lundstrom, Surface and perimeter recombination in GaAs diodes: an experimental and theoretical investigation, IEEE Transactions on Electron Devices 38 (1991) 1253–1261.

[3] B. Mazhari, H. Morkoc, Surface recombination in GaAs PN junction diode, Journal of Applied Physics 73 (1993) 7509–7514.

[4] A. Belghachi, S. Khelifi, Modelling of the perimeter recombination effect in GaAs-based micro-solar cell, Solar Energy Materials and Solar Cells 90 (2006) 1–14.

[5] H. Atwater, Paths to high efficiency low-cost photovoltaics, in: Photovoltaic Specialists Conference (PVSC), 2011 37th IEEE, pp. 1–3.

[6] M. Sheldon, C. Eisler, H. Atwater, GaAs Passivation with Trioctylphosphine Sulfide for Enhanced Solar Cell Efficiency and Durability, Advanced Energy Materials, 2 (2012) 339-344.

[7] S. Sze, Physics of semiconductor devices, Wiley, 1981, 96.

[8] C.H. Henry, R.A. Logan, F.R. Merritt, The effect of surface recombination on current in $Al_xGa_{1-x}As$ heterojunctions, Journal of Applied Physics 49 (1978) 3530–3542.

[9] S. Tiwari, D.J. Frank, S.L. Wright, Surface recombination in GaAlAs/GaAs heterostructure bipolar transistors, Journal of Applied Physics 64 (1988) 5009–5012.

[10] Atlas user's manual, Device Simulation Software, Silvaco International, 2012.

[11] M. Levinshtein, S. Rumyantsev, M. Shur, Handbook Series on Semiconductor Parameters, vol. 1, World Scientific, 1996.

[12] M. Levinshtein, S. Rumyantsev, M. Shur, Handbook Series on Semiconductor Parameters, vol. 2, World Scientific, 1999.

[13] S. Jain, J. McGregor, D. Roulston, P. Balk, Modified simple expression for bandgap narrowing in n-type GaAs, Solid-State Electronics 35 (1992) 639–642.

[14] R. Ahrenkiel, M. Lundstrom, Minority Carriers in III–V Semiconductors: Physics and Applications, vol. 39, Academic Press, 1993.

[15] D. Klaassen, A unified mobility model for device simulation I. Model equations and concentration dependence, Solid-State Electronics 35 (1992) 953–959.

[16] D. Klaassen, A unified mobility model for device simulation II. Temperature dependence of carrier mobility and lifetime, Solid-State Electronics 35 (1992) 961–967.

[17] M. Sotoodeh, A. Khalid, A. Rezazadeh, Empirical low-field mobility model for III–V compounds applicable in device simulation codes, Journal of Applied Physics 87 (2000) 2890.

[18] M. Klausmeier-Brown, M. Lundstrom, M. Melloch, S. Tobin, Effects of heavy impurity doping on electron injection in p^+–n GaAs diodes, Applied Physics Letters 52 (1988) 2255–2257.

[19] D. Caughey, R. Thomas, Carrier mobilities in silicon empirically related to doping and field, Proceedings of the IEEE 55 (1967) 2192–2193.

[20] P. DeMoulin, The physics and modeling of gallium arsenide solar cells (1988). ProQuest Dissertations and Theses, 194 p. Retrieved from ⟨http://search.proquest.com/docview/303592299?accountid=14712⟩.

[21] J.G. Simmons, G.W. Taylor, Nonequilibrium steady-state statistics and associated effects for insulators and semiconductors containing an arbitrary distribution of traps, Physical Review B 4 (1971) 502–511.

[22] P. Ciampolini, A. Pierantoni, M. Melanotte, C. Cecchetti, C. Lombardi, G. Baccarani, Realistic device simulation in three dimensions [EPROM cell], in: International Electron Devices Meeting, 1989. IEDM '89. Technical Digest, pp. 131–134.

[23] K. Tomizawa, Numerical Simulation of Submicron Semiconductor Devices, Artech House Boston, 1993.

[24] N. Goto, Y. Ohno, H. Yano, Two-dimensional numerical simulation of side-gating effect in GaAs MESFETs, IEEE Transactions on Electron Devices 37 (1990) 1821–1827.

[25] P. Dodd, Studies of Heterojunction Bipolar Transistor Device Physics and New Device Concepts, Ph.D. Thesis, 1993.

[26] Deckbuild user's manual, Device Simulation Software, Silvaco International, 2012.

[27] W. Mönch, Semiconductor Surfaces and Interfaces, vol. 26, Springer, 2001.

[28] C. Algora, Very-high-concentration challenges of III–V multijunction solar cells, Concentrator Photovoltaics 130 (2007) 89–111. (Springer Series in Optical Sciences Volume 130).

[29] T. Stellwag, M. Melloch, M. Lundstrom, M. Carpenter, R. Pierret, Orientation-dependent perimeter recombination in GaAs diodes, Applied Physics Letters 56 (1990) 1658–1660.

[30] V. Díaz, C. Algora, Effects of the size and shape of GaAs solar cells on recombination losses, in: Actas 3ra. Conferencia Dispositivos Electrónicos (2001) 289–292.